Brodogradnja Volume 77 Number 1 (2026) 77101

University of Zagreb
Faculty of Mechanical
Engineering and Naval
Architecture

journal homepage: www.brodogradnja.fsb.hr

Brodogradnja

An International Journal of Naval Architecture and
Ocean Engineering for Research and Development

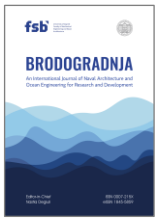

Marine engine cylinder exhaust temperature prediction based on PSO-optimized CNN-LSTM-attention network

Yang Cao[1], *Jundong Zhang*[1, 2, *], *Ao Ma*[1], *Hongbo Xu*[1], *Jiale Liu*[1]

[1]*Marine Engineering College, Dalian Maritime University, Dalian 116026, China*
[2]*Dalian Maritime University Smart Ship Limited Company, Dalian 116026, China*

ARTICLE INFO

Keywords:
Marine engine
Exhaust temperature prediction
CNN-LSTM-Attention model
Particle swarm optimization

ABSTRACT

Marine diesel engines play a critical role in ensuring vessel safety and stable operation. Among their operating parameters, cylinder exhaust gas temperature is a key indicator of an engine's thermal performance and overall health. Accurate forecasting of this parameter is therefore essential for real-time monitoring and condition-based maintenance in intelligent ship propulsion systems. This study proposes a hybrid CNN-LSTM-Attention model for long-range prediction of marine engine cylinder exhaust temperature. The model utilizes real-world sensor data acquired from shipboard monitoring systems, rather than synthetic or simulated datasets. Experimental results demonstrate the model's superior performance, achieving a Mean Absolute Error (MAE) of 3.9944, a Mean Absolute Percentage Error (MAPE) of 1.3481 %, and a coefficient of determination (R^2) of 0.9805. These metrics indicate high prediction accuracy and minimal deviation from actual values compared to conventional algorithms. To further enhance the model's predictive capability and generalization performance, Particle Swarm Optimization (PSO) was applied. This automatically fine-tune key hyperparameters, including the optimal parameter settings for learning rate and the number of LSTM units. Results confirm that PSO optimization improves the CNN-LSTM-Attention model's predictive performance. The predicted temperature curves align better with actual measurements. Specifically, the MAE was reduced by 1.5431, the MSE decreased by 14.3743, and the R^2 value moved closer to 1. Leveraging PSO's self-adaptive search capability avoided the need for complex manual hyperparameter tuning. Overall, the findings confirm that the optimized model delivers highly accurate predictions of cylinder exhaust temperature in intelligent marine engines.

1. Introduction

The rapid advancement of science, technology, and artificial intelligence has substantially accelerated the development and construction of intelligent ships [1] have progressed substantially in recent years. This technological evolution has attracted growing attention from academic researchers and stakeholders within the maritime industry. Intelligent ships represent the convergence of conventional marine engineering with

* Corresponding author.
E-mail address: zhjundong@dlmu.edu.cn

https://doi.org/10.21278/brod77101
Received 21 April 2025; Received in revised form 8 June 2025; Accepted 6 August 2025
Available online 16 August 2025
ISSN 0007-215X; eISSN 1845-5859

emerging disciplines encompassing artificial intelligence, information processing, and autonomous systems [2, 3]. Research endeavors in this domain spans a diverse range of topics, ranging from environmental modeling [4], optimal route planning [5], autonomous navigation [6], and collision avoidance [7].

The inherent complexity and variability of marine operations necessitate the analysis of onboard system data for accurate assessment of ship performance and navigational safety assurance. Examining both real-time voyage data and historical records facilitates the identification of potential mechanical faults and irregularities in critical operational parameters [8, 9]. These insights support the application of preventive maintenance strategies, enabling timely actions [10] - such as part inspection, repair, or replacement. It can contribute to improved reliability, operational safety, and lifecycle health management of vessels.

Modern smart ships deploy extensive arrays of sensors and monitoring units, perpetually generating vast volumes of time-series and multidimensional data. The size and complexity of these datasets make manual interpretation inefficient and error prone. Therefore, it has become increasingly necessary to adopt advanced models and intelligent algorithms for condition monitoring and fault forecasting has become increasingly necessary. In particular, automated analysis not only reduces manual workload but also improves diagnostic accuracy and predictive efficiency [11, 12].

Advancements in deep learning have significantly revolutionized predictive modelling precision and robustness of predictive modelling in marine propulsion systems. Numerous studies have investigated the application of neural networks - particularly convolutional and recurrent architectures - in forecasting critical engine parameters such as exhaust gas temperature, cylinder pressure, turbocharger speed, and lubrication conditions. Wang et al. [13] introduced an enhanced ECA-ICNN model for diesel engine fault diagnosis, incorporating an adaptive mechanism to augment CNN structure flexibility and diagnostic efficacy. This architecture efficiently captured inter-feature dependencies while achieving promising diagnostic accuracy. Sun et al. [14] developed a multi-layer attention-based hybrid CNN-LSTM-MLA framework that accounts for various real-world operating conditions to improve marine diesel engines exhaust gas temperature prediction. Meanwhile, Liu et al. [15] advanced fault prognostics through a bidirectional gated recurrent unit (BiGRU) architecture, enabling early stage detection of abnormal engine behavior.

Ji et al. [16] proposed a CNN-BiLSTM-Attention model for ship diesel engine exhaust temperature prediction. Their methodology integrated Mahalanobis distance transformation to establish a quantitative EGT monitoring index with defined thresholds and alarm levels. Experimental results demonstrated the model's efficacy in detecting early-stage fault patterns and generating timely warnings. Furthermore, Han et al. [17] implemented a LSTM based fault prediction networks, validating its performance using hybrid power laboratory data. Patil et al. [18] proposed a swarm-based Cauchy Particle Swarm Optimization method for hyperparameter tuning of LSTM temperature prediction models. Collectively, these advances indicate that deep learning models–particularly hybrid CNN–LSTM–Attention frameworks– exhibit significant potential for intelligent parameter forecasting and anomaly detection in marine propulsion systems.

Building on these advances, this study focuses on the No. 1 WÄRTSILÄ 8L20 diesel engine installed aboard the *Xin Hong Zhuan* intelligent vessel. We propose a deep learning model integrating a PSO-optimized CNN-LSTM-Attention architecture [19] is proposed to forecast the engine cylinder exhaust temperature under various operating conditions. The model is trained on real data [20] collected by intelligent sensors [21] during actual voyages, capturing both spatial features and temporal dependencies embedded in the operational signals [22].

The CNN-LSTM-Attention model demonstrates significant advancements in predicting cylinder exhaust temperature trends, outperforming conventional approaches. Specifically, comparative analysis against LSTM, CNN-LSTM, and LSTM-Attention baselines reveal quantified enhancements: Mean Absolute Error (MAE) reductions of 2.7394, 4.3334, and 2.9826, coupled with Mean Squared Error (MSE) decreases of 104.9556, 81.6197, and 39.8867 respectively. The proposed model demonstrates commanding superiority across all evaluation metrics, achieving higher accuracy with reduced prediction errors. Integrating PSO enable the automatic fine-tuning of key hyperparameters - particularly learning rate and LSTM units count. This enhancement directly improves the model's adaptability to diverse engine operating conditions, strengthens its generalization capability, and ensures stable performance consistency across scenarios. The

optimized model further demonstrates strong reliability with real-world operational data, confirming its practical applicability for intelligent engine monitoring and early fault detection in vessel systems.

The findings offer meaningful theoretical and practical contributions to intelligent ship condition monitoring [23]. By enabling accurate real-time assessment of engine thermal behavior, the proposed framework supports informed decision-making by onboard operators and maintenance personnel [24]. This predictive capability is crucial for mitigating issues–including incomplete combustion, engine components overheating, and turbocharger malfunctions which can trigger abnormal exhaust temperature patterns and compromise propulsion safety. Ultimately, the deployment of intelligent forecasting models contributes to ensuring the stable, healthy operation of marine propulsion systems [25] and promotes the safe [26, 27] and navigation efficiency in next-generation intelligent vessels.

This paper is structured as follows. Section 2 delineates the fundamental components of the CNN-LSTM-Attention model, elaborating on the rationale and advantages of this hybrid architecture for marine engine exhaust temperature prediction. Section 3 provides a technical overview of the *Xin Hong Zhuan* vessel, highlighting its principal specifications while detailing real-world sensor data acquisition, preprocessing methodologies, and key parameter configuration. Section 4 presents the implementation for exhaust temperature prediction using the CNN-LSTM-Attention network, accompanied by comparative analysis against conventional algorithms. The results validate the proposed model's exceptional accuracy in forecasting exhaust gas temperature. Building on this, the section further details the integration of PSO to enhance the baseline model, achieving significant improvements in prediction precision, computational efficiency, and generalization capability. Finally, section 5 summarizes the principal findings, highlights methodological contributions, and discusses limitations along with future research directions.

2. Deep learning model theory

2.1 Convolutional Neural Network (CNN)

Convolutional Neural Network is widely utilized for the extraction of spatial features from sequential or grid-structured data [28, 29]. Through the process of dimensionality reduction during data preprocessing, CNN can decrease the total number of trainable parameters and network weights. It also can reduce the model complexity and the risk of overfitting [30]. This contributes to a more streamlined and efficient training process and enhances overall model performance [31, 32]. The standard architecture of a CNN typically consists of the following five key components:

(a) Input Layer

The input layer is responsible for receiving raw data and representing each input as a distinct feature [33]. These features are subsequently passed through the network for hierarchical processing.

(b) Convolutional Layer

As the core component of the CNN, the convolutional layer [34] extracts local spatial features from the input data by applying convolutional operations. Each convolutional layer contains multiple filters (also known as kernels), which vary in size and depth depending on the network design. The kernel values are initialized randomly and iteratively updated during training via backpropagation to enhance feature extraction capability.

(c) Pooling Layer

The pooling layer performs spatial down sampling to reduce the resolution of the feature maps generated by the convolutional layers. This step helps to preserve the most salient information, reduce the computational burden, and suppress overfitting. Common pooling strategies include max pooling and average pooling, which respectively select the maximum or mean value within a localized region.

(d) Fully Connected Layer

Following the convolutional and pooling stages, the fully connected layer transforms the multidimensional feature maps into a one-dimensional feature vector. Each neuron in this layer is connected to every neuron in the preceding layer. The Rectified Linear Unit (ReLU) [35] activation function is commonly

used to introduce nonlinearity and enhance learning capacity. This layer aggregates and integrates local features to facilitate final classification or regression decisions.

(e) Output Layer

The output layer typically employs the Softmax activation function to convert the output vector from the fully connected layer into a probability distribution over predefined target classes [36]. The resulting values represent the final predictions of the network.

The overall architecture of a CNN is depicted schematically in Figure 1, which illustrates the hierarchical flow of data from raw input to final output through successive layers of transformation.

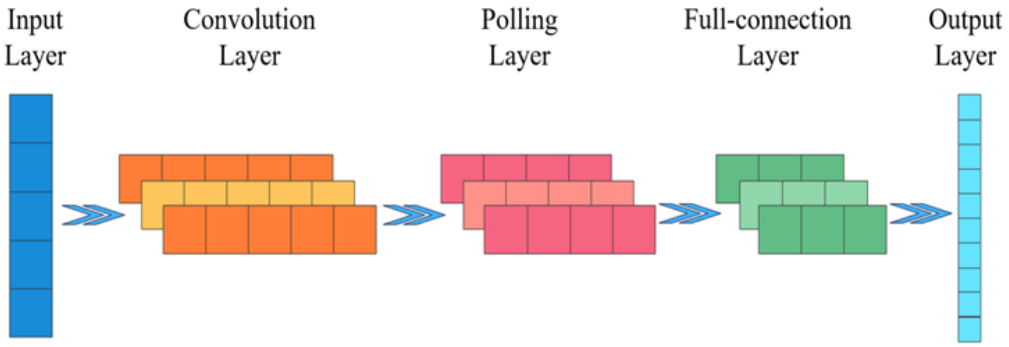

Fig. 1 CNN neural network structure diagram.

2.2 Long Short Term Memory (LSTM)

The Long Short-Term Memory network is a specialized type of Recurrent Neural Network (RNN). It is designed to address the limitations of traditional RNN, particularly their difficulty in capturing long-term dependencies in sequential data. As illustrated in Figure 2, LSTM introduces a gated mechanism [37] and a dedicated memory cell [38] to regulate information flow across time steps. These architectural enhancements allow the model to selectively retain, discard, or update information. Then it can significantly improve its ability to learn long-range temporal patterns and global contextual relationships.

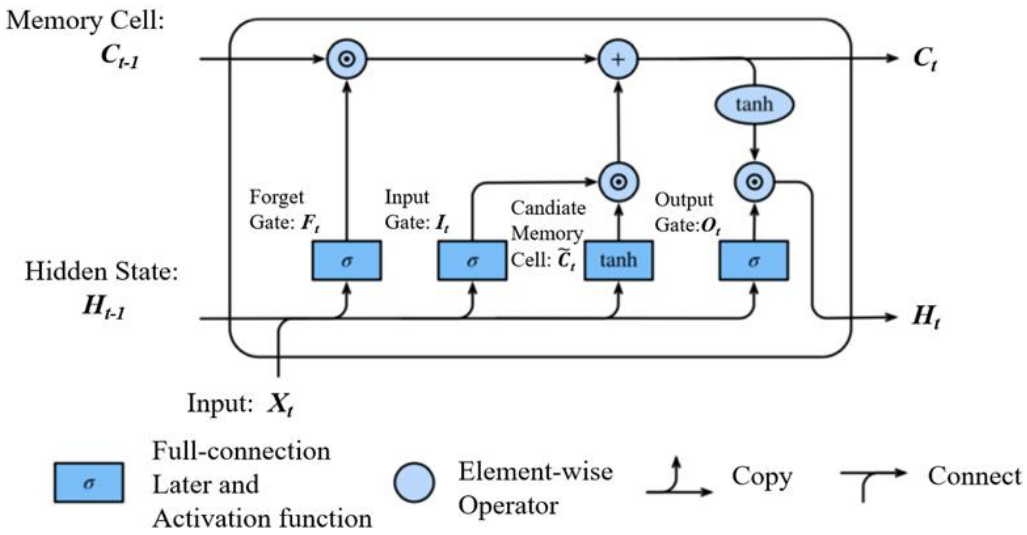

Fig. 2 Schematic diagram of LSTM neural network.

LSTM processes sequential data through a chain-like structure, where each unit - referred to as an LSTM cell or memory block - corresponds to a discrete time step [39]. At each time step t, the network receives an

input vector x_t and the hidden state from the previous time step h_{t-1}. Based on this information, the memory cell state and the hidden state are updated through the following procedures:

(a) Forget Gate

The forget gate determines which information from the previous memory cell state c_{t-1} should be discarded [40]. The gate's activation is computed as:

$$F_t = \sigma\left(\boldsymbol{W}_f \cdot [h_{t-1}, x_t] + b_f\right) \tag{1}$$

where W_f denotes the weight matrix associated with the forget gate; b_f is the bias term for the forget gate; The sigmoid activation function $\sigma(\cdot)$ ensures that the output lies in the range (0,1), enabling partial retention or complete removal of prior memory content.

(b) Input Gate

The input gate [40] governs the incorporation of new information into the cell state. It consists of two parts: the update gate $I(t)$ and the candidate memory vector $\tilde{C}_t$, computed as:

$$I_t = \sigma(\boldsymbol{W}_i \cdot [h_{t-1}, x_t] + b_i) \tag{2}$$

$$\tilde{C}_t = \tanh(\boldsymbol{W}_c \cdot [h_{t-1}, x_t] + b_c) \tag{3}$$

where W_i: the weight for the input gate; b_i: the bias for the input gate. W_c: the weight for the candidate memory content; b_c: the parameters for the candidate memory content.

The updated memory cell state is then obtained by combining the output of the forget and input gates:

$$C_t = F_t \odot c_{t-1} + I_t \odot \tilde{C}_t \tag{4}$$

$\odot$ denotes element-wise multiplication.

(c) Output Gate

The output gate controls how much of the cell state is exposed as the hidden state [40]. Its activation is computed as:

$$O_t = \sigma(\boldsymbol{W}_o \cdot [h_{t-1}, x_t] + b_o) \tag{5}$$

The hidden state H_t is then computed as the element-wise product of the output gate and the activated memory cell:

$$H_t = O_t \odot \tanh(C_t) \tag{6}$$

where W_o: the weight matrix associated with the output gate; b_o: the bias for the output gate.

The resulting H_t serves as both the output of the current LSTM unit and the input to the next time step, effectively capturing both current and historical temporal dynamics.

2.3 Attention Mechanism

The attention mechanism [41] has become a key element in deep learning, particularly in models that handle sequential data. Inspired by human cognitive behavior, it allows the model to focus on the most relevant parts of the input while reducing the effect of less important information [42]. This selective weighting helps the network capture long-term dependencies, improves accuracy, and enhances interpretability. Due to these advantages, attention-based models have gained widespread adoption in fields such as natural language processing, speech recognition, image analysis, and time-series forecasting.

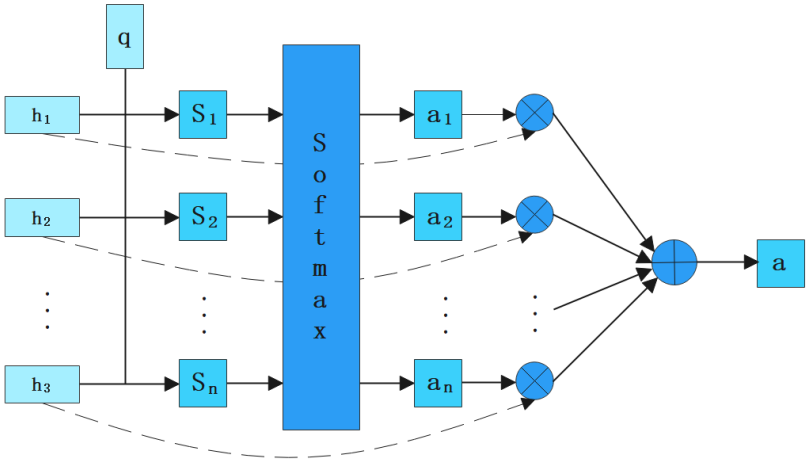

Fig. 3 Attention mechanism structure diagram.

As depicted in Figure 3, the attention mechanism generally comprises three core components: (1) the input representations (queries, keys, and values); (2) the computation of attention scores (or weights); (3) the formation of a context vector via weighted summation. At the core of the mechanism lies the idea of computing a relevance score, which reflects the relationship between each element of the input and a specific point in the output sequence.

The computation process [43] can be summarized in the following steps:

(a) Score Computation

Given a query vector (e.g., the decoder hidden state s_{t-1}) and a set of key vectors (e.g., encoder hidden states h_t), the attention score is computed to measure the relevance between them:

$$\alpha(s_{t-1}, h_t) = \vartheta_a^T \tanh(W_h h_t + W_s s_{t-1} + b) \tag{7}$$

where $\alpha(s_{t-1}, h_t)$ denotes the alignment score, indicating the importance of the encoder hidden state h_t at time step t with respect to the decoder's previous hidden state s_{t-1}. ϑ_a^T is a learnable weight vector that transforms the combined representation into a scalar score, while W_h and W_s are trainable weight matrices, and b is a bias term.

(b) Normalization

The raw attention scores are normalized using a Softmax function to produce attention weights that sum to one across all time steps:

$$\alpha_t = \frac{\exp\big(\alpha(s_{t-1}, h_t)\big)}{\sum_{t=1}^{T} \exp\big(\alpha(s_{t-1}, h_t)\big)} \tag{8}$$

This ensures that the attention weights sum to one and can be interpreted as the importance of each encoder state relative to the current decoding context.

(c) Context Vector Calculation

Finally, a context vector is generated by computing a weighted sum of the encoder hidden states using the normalized attention weights:

$$Att = \sum_{t=1}^{n} \alpha_t h_t \tag{9}$$

The context vector Att encapsulates the most relevant temporal and contextual information, conditioned on the current decoder state. This dynamically updated representation enhances the model's ability to focus on informative segments of the input sequence, thereby improving performance in sequential prediction tasks such as exhaust temperature forecasting in marine engines.

2.4 CNN-LSTM-Attention Network Model

Based on the integration of three core deep learning methods - Convolutional Neural Network, Long Short-Term Memory, and the Attention mechanism - a hybrid prediction model is developed, as shown in Figure 4. This combined CNN-LSTM-Attention model [44] is designed to improve the accuracy and reliability of time-series forecasting, with a focus on predicting exhaust gas temperature in marine engine cylinders.

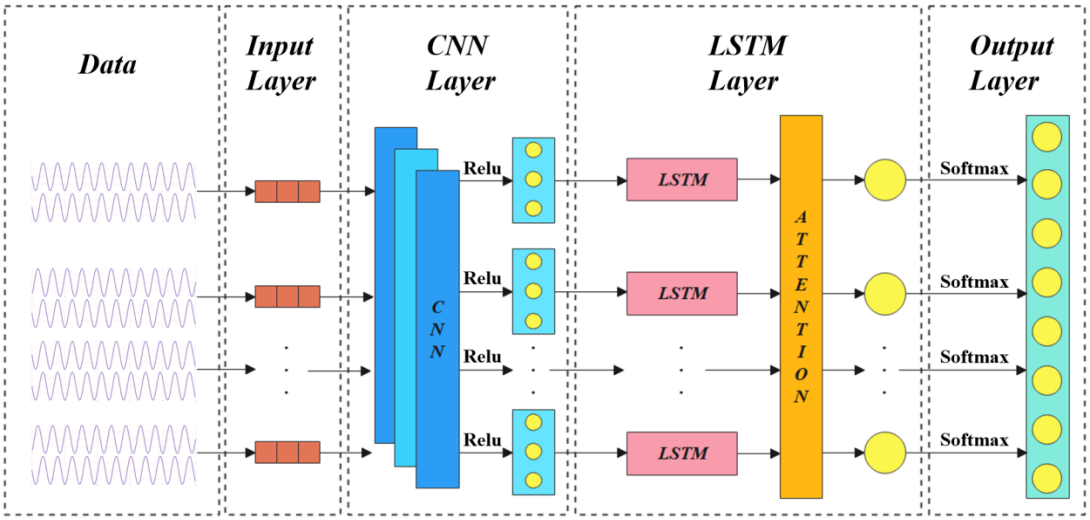

Fig. 4 CNN-LSTM-Attention network model.

The integration of the Attention mechanism into the CNN-LSTM framework allows the model to emphasize spatial features that are most relevant to the prediction task. By assigning greater weight to critical features extracted by the CNN, the LSTM component can focus more effectively on key temporal patterns during sequence [45] processing. This enhancement improves both the interpretability and predictive accuracy of the model.

The data processing workflow of the CNN-LSTM-Attention model is structured in five sequential steps:

(a) Sequence Formatting

The initial stage involves converting the raw time-series data collected from onboard sensors into a matrix format suitable for neural network input. This transformation includes applying temporal segmentation and normalization techniques to ensure consistency and enhance the effectiveness of subsequent feature extraction processes.

(b) Feature Extraction via CNN

The preprocessed matrix is input into the CNN module [46], where convolutional and pooling operations are applied to extract local patterns and reduce data dimensionality. These layers capture short-term correlations and spatial dependencies in the data.

(c) Temporal Modeling via LSTM

The sequential features obtained from the CNN are fed into the LSTM layer [46]. Here, long-term temporal dependencies are learned, enabling the model to understand evolving patterns in the data - such as gradual increases or anomalies in cylinder exhaust temperature over time.

(d) Attention-Based Weighting

The output from the LSTM layer is passed to the Attention mechanism, which calculates attention weights and performs a weighted summation of hidden states. This step allows the model to emphasize time steps that are most critical to the current prediction, enhancing the model's focus and interpretive accuracy.

(e) Final Prediction via Fully Connected Layer

The resulting attention-weighted feature vector is passed through a fully connected layer, where a final prediction is generated. A Softmax activation function is typically applied when multi-class classification is

involved, although for regression tasks, a linear activation may be used. The final output is then visualized or used for decision-making in intelligent maintenance systems.

Marine diesel engines operate under highly dynamic and nonlinear conditions, where single-model approaches often struggle to balance local feature extraction and long-term sequence learning. The decision to adopt the CNN-LSTM-Attention network for predicting marine engine exhaust temperature is based on the need to effectively capture the complex spatial–temporal dependencies present in engine operation data. CNN networks can identify local spatial correlations among multiple input parameters, such as pressure, temperature, and rotational speed. LSTM networks provide the ability to model time-dependent behaviours and detect long-range temporal trends. By incorporating an Attention mechanism, the model further enhances its ability to selectively focus on the most relevant features and time steps, which is especially valuable in the context of fluctuating marine environments. Together, these components form a robust framework that offers improved accuracy, adaptability, and interpretability for predictive tasks involving exhaust gas temperature in intelligent marine propulsion systems.

3. Deep learning model theory

3.1 Data Collection

The *Xin Hong Zhuan* is an intelligent vessel designed for both research and training purposes. The vessel has a length overall of 69.83 meters, a beam of 10.9 meters, and a depth of 5.0 meters. It is designed for a cruising speed of 18 knots and has a displacement of 1430 tons. The propulsion system comprises two fully electric azimuth thrusters, each rated at 1500 kW. It is powered by three 1520 kW diesel generator sets. Additionally, the vessel is equipped with a bow thruster and anti-roll fins, enabling a maximum range of up to 2500 nautical miles. The *Xin Hong Zhuan* is recognized as the intelligent training and research ship equipped with autonomous navigation, remote control, and independent operation capabilities. It serves as a mobile experimental platform for testing and validating smart ship technologies at sea.

This study selects the vessel's No.1 main diesel engine, specifically the WÄRTSILÄ 8L20 model, as the primary research object. This engine is extensively instrumented with real-time sensors, featuring more than 15,000 monitoring and control points, which is approximately 30 times greater than that of conventional ships. These sensors enable continuous acquisition and logging of key operational parameters, including exhaust temperature, fuel injection timing, rotational speed, and various pressure levels. A summary of the engine's main technical specifications is provided in Table 1.

Table 1 Main specifications of the WÄRTSILÄ 8L20 engine onboard Xin Hong Zhuan.

Engine Parameter	Unit	Value
Cylinder bore	mm	200
Number of cylinders	/	8
Rated power	kW	1600
Rated speed	rpm	1000
Piston displacement per cylinder	l	8.80
Stroke length	mm	280
Clockwise firing order	/	1-3-7-4-8-6-2-5

To facilitate accurate data acquisition under real-world maritime conditions, the WÄRTSILÄ 8L20 engine is instrumented with multiple sensor types, including exhaust temperature sensors, cylinder pressure sensors, crankshaft speed sensors, and intake or exhaust manifold pressure sensors. A schematic illustration of selected sensor installations is provided in Figure 5. In this figure, sensors numbered 1 to 8 represent cylinder pressure sensors mounted at the indicator valve positions. Sensors 9 and 10 are speed sensors installed on brackets facing the engine flywheel. These sensors [47] are strategically deployed at key engine locations to capture high-resolution data during periods of stable engine operation. Sensor readings are collected at fixed

sampling intervals and transmitted to a local data management platform, thereby forming a time-continuous and high-dimensional dataset. This dataset forms the basis for the model development and performance evaluation in the predictive maintenance framework proposed in this work.

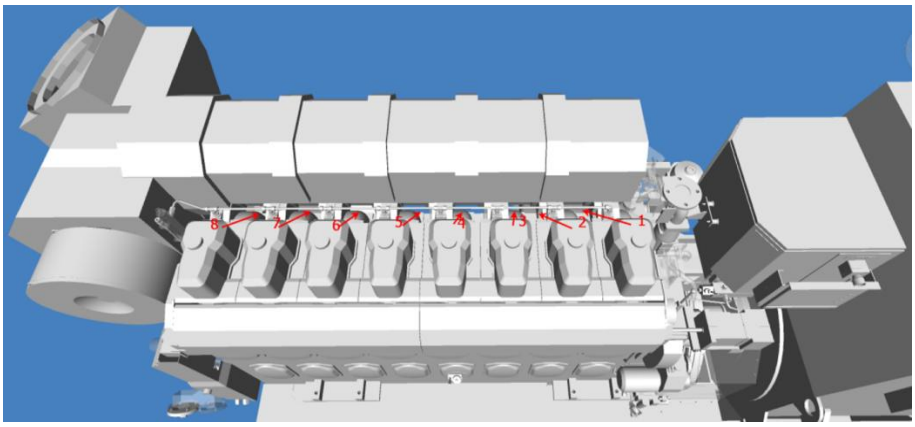

(a) Pressure Sensors

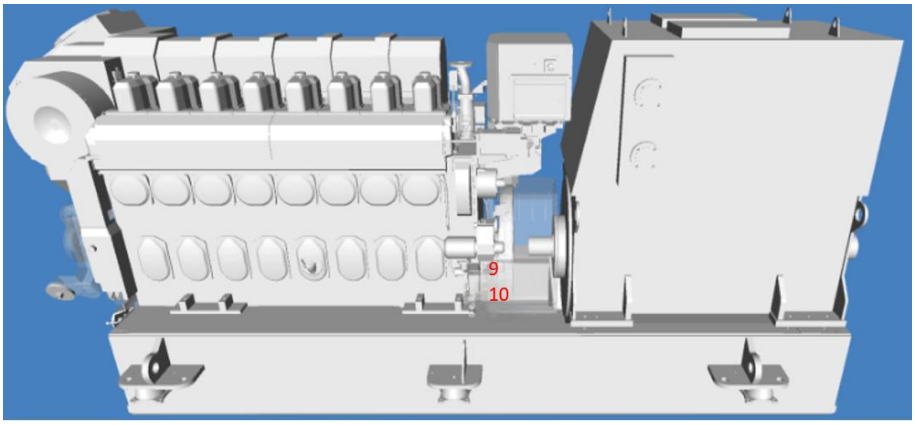

(b) Speed Sensors

Fig. 5 Schematic illustration of selected sensor installations on the main engine.

Table 2 Monitored feature parameters from smart sensors.

Parameter Description	Unit	Symbol
Average cylinder exhaust temperature of Engine No. 1	℃	T_P
Lubricating oil inlet temperature of Engine No. 1	℃	T_1
Cylinder liner cooling water inlet temperature of Engine No. 1	℃	T_2
Cylinder liner cooling water outlet temperature of Engine No. 1	℃	T_3
Turbocharger exhaust inlet temperature of Engine No. 1	℃	T_4
Turbocharger exhaust outlet temperature of Engine No. 1	℃	T_5
Fuel inlet pressure of Engine No. 1	bar	P_1
Lubricating oil inlet pressure of Engine No. 1	bar	P_2
Engine speed of Engine No. 1	rpm	N_1
Turbocharger speed of Engine No. 1	rpm	N_2

The No. 1 main engine of the *Xin Hong Zhuan* vessel is equipped with eight cylinders. Therefore, in this study, the average exhaust gas temperature of all eight cylinders which is recorded under normal operating conditions is used as the practical reference value for predictive analysis. Due to the large volume of data generated during actual voyage operations, a feature selection and preprocessing phase was implemented to

streamline the dataset. Based on a review of relevant literature and manufacturer documentation, nine key influencing parameters were identified to exhibit significant correlation with exhaust temperature. These include engine speed, lubricating oil inlet pressure, turbocharger inlet and outlet temperatures, cylinder liner cooling water temperatures, and lubricating oil inlet temperature, among others.

In total, approximately 300,000 raw data entries were collected through the intelligent sensor system installed onboard. A detailed summary of the monitored parameters and representative samples of the original dataset are provided in Table 2.

3.2 Data Analysis

To evaluate the relationship between key engine parameters, this study applies the Spearman rank correlation method. As a non-parametric statistical tool, Spearman's correlation [48] does not require the data to follow a normal distribution or exhibit linear relationships. This makes it especially suitable for analyzing non-linear data and datasets with outliers.

The Spearman correlation coefficient, denoted as r_s, measures the strength and direction of a monotonic association between two variables. It is calculated using the following equation:

$$r_s = 1 - \frac{6\sum_{i=1}^{n} d_i^2}{n(n^2-1)} \tag{10}$$

where d_i represents the rank difference between two variables for the $i-th$ observation, and n is the total number of observations. The coefficient r_s [49] ranges between −1 and 1, where values closer to 1 or −1 indicate strong positive or negative monotonic relationships, respectively.

To aid in interpreting the correlation results, the strength of association was categorized based on the guideline presented in Table 3. This classification framework facilitates a systematic evaluation of variable interactions in the dataset.

Table 3 Classification of correlation strength based on absolute value of Spearman's rank correlation coefficient $|r_s|$.

$\|r_s\|$ Range	Correlation Strength
$0.8<\|r_s\|\leq 1$	Very strong correlation
$0.6<\|r_s\|\leq 0.8$	Strong correlation
$0.4<\|r_s\|\leq 0.6$	Moderate correlation
$0.2<\|r_s\|\leq 0.4$	Weak correlation
$0\leq\|r_s\|\leq 0.2$	Negligible correlation

In the present study, the Spearman method was applied to the dataset described in Section 3.1 to explore dependencies among nine key operational parameters influencing exhaust gas temperature. To further improve interpretability, a correlation heatmap [50] was generated and is depicted in Figure 6. In the heatmap, colour intensity corresponds to the magnitude of the correlation coefficient: warmer colours (e.g., red) represent stronger correlations, while cooler colours (e.g., blue) indicate weaker relationships. This visualization provides an intuitive representation of how individual parameters affect exhaust temperature, thereby supporting feature selection and subsequent modelling decisions for predictive analysis.

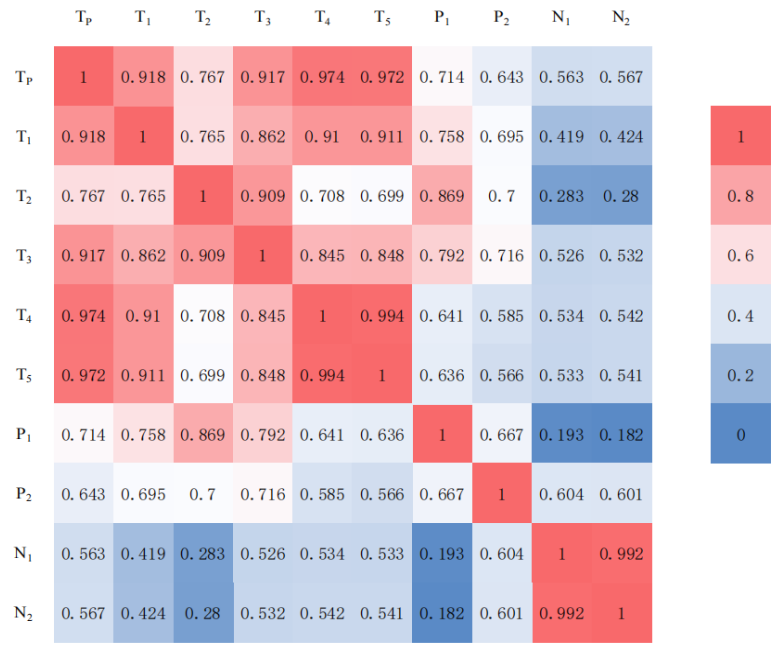

Fig. 6 Heatmap visualization of Spearman correlation coefficients among key engine parameters.

3.3 Data Preprocessing

To improve the accuracy of the prediction results and minimize model error, a data filtering process was applied based on the degree of correlation between feature variables and the target variable - cylinder exhaust temperature (T_P). Specifically, features with relatively low correlation coefficients were excluded to construct a refined dataset for model training and prediction.

As shown in Figure 6, among the nine examined variables, the turbocharger exhaust inlet temperature (T_4) demonstrated the highest positive correlation with the average cylinder exhaust temperature, with a correlation coefficient of 0.974. In contrast, engine speed (N_1) showed the weakest correlation, with a coefficient of 0.563. Based on this correlation analysis, three parameters - N_1, turbocharger speed (N_2), and lubricating oil inlet pressure (P_2) - were excluded from the final dataset, as their correlation coefficients were below the threshold of 0.700.

Table 4 Representative records from the filtered dataset used for model training and evaluation.

T_P	T_1	T_2	T_3	T_4	T_5	P_1
268.19	64.7	85.3	86.9	281.2	264.4	7.33
268.49	64.7	85.3	86.9	281.7	264.6	7.34
268.60	64.7	85.3	86.8	281.7	264.9	7.35
...	...	...	...	...	...	...
371.31	64.4	82.4	86.9	486.9	368.8	6.60
371.61	64.5	82.4	86.9	486.9	368.8	6.60
371.54	64.6	82.5	86.9	487.0	368.8	6.61
...	...	...	...	..	...	...
237.91	63.5	83.2	84.6	266	271.9	7.31
237.98	63.5	83.2	84.6	264.9	269.9	7.31
237.98	63.5	83.3	84.6	263.2	267.7	7.33

The remaining six parameters, each exhibiting a correlation value above 0.700, were retained. These included T_4, lubricating oil inlet temperature (T_1), and four other relevant features. Together with the target variable T_P, they were used to construct a refined dataset for model development. After filtering, approximately 140,000 valid data samples were obtained from the operational records of the No. 1 main engine under steady-state conditions, providing a reliable foundation for predictive analysis.

From this dataset, a subset of 10,000 representative records was selected for the training and validation of the proposed deep learning model. The selected data samples reflect a wide range of real-world engine operating scenarios. And it ensures the robustness and applicability of the resulting model. The excerpt from the preprocessed dataset, including key parameter values, is presented in Table 4.

3.4 Optimal Hyperparameter Configuration

To assess the performance of the proposed model in predicting marine engine cylinder exhaust temperature, both graphical and numerical approaches were used. In addition to visually comparing the overlap between the predicted and actual value curves, the study also analyzed numerical error metrics [51] are applied.

The evaluation criteria include the following indicators:

(a) Mean Absolute Error (MAE).
(b) Mean Square Error (MSE).
(c) Root Mean Square Error (RMSE).
(d) Mean Absolute Percentage Error (MAPE).
(e) The Coefficient of Determination (R^2).

The calculation formulas for each metric are shown below:

$$MAE = \frac{1}{n}\sum_{i=1}^{n}|\hat{y}_i - y_i|\ ,\ \ \epsilon[0,+\infty) \tag{11}$$

$$MSE = \frac{1}{n}\sum_{i=1}^{n}(\hat{y}_i - y_i)^2\ ,\ \ \epsilon[0,+\infty) \tag{12}$$

$$MAPE = \frac{100\%}{n}\sum_{i=1}^{n}\left|\frac{\hat{y}_i - y_i}{y_i}\right|\ ,\ \ \epsilon[0,+\infty) \tag{13}$$

$$RMSE = \sqrt{MSE} = \sqrt{\frac{1}{n}\sum_{i=1}^{n}(\hat{y}_i - y_i)^2}\ ,\ \ \epsilon[0,+\infty) \tag{14}$$

Each formula includes specific physical quantities that represent predicted and observed values: $\hat{y}_i$: this refers to the model's output for the $i-th$ predicted value. y_i: this is the actual measured value from sensor data for the $i-th$ sample. n: the total number of data points or observations used in the evaluation.

The dataset was randomly divided into three parts. These included training, validation, and testing sets, following a 7:2:1 ratio. The training set was used to fit the model. The validation set helped in adjusting the model's hyperparameters. During training, performance on the validation data was closely observed. The model configuration that produced the lowest prediction error and best matched the actual values was selected.

To evaluate the impact of the forecast horizon (output step size) on model performance, several output step configurations were tested. The results are visualized in Figure 7, which shows that as the output step size increases, the degree of overlap between predicted and actual curves deteriorates. When the output step is set to 1, the model achieves the highest fidelity in capturing real-time trends.

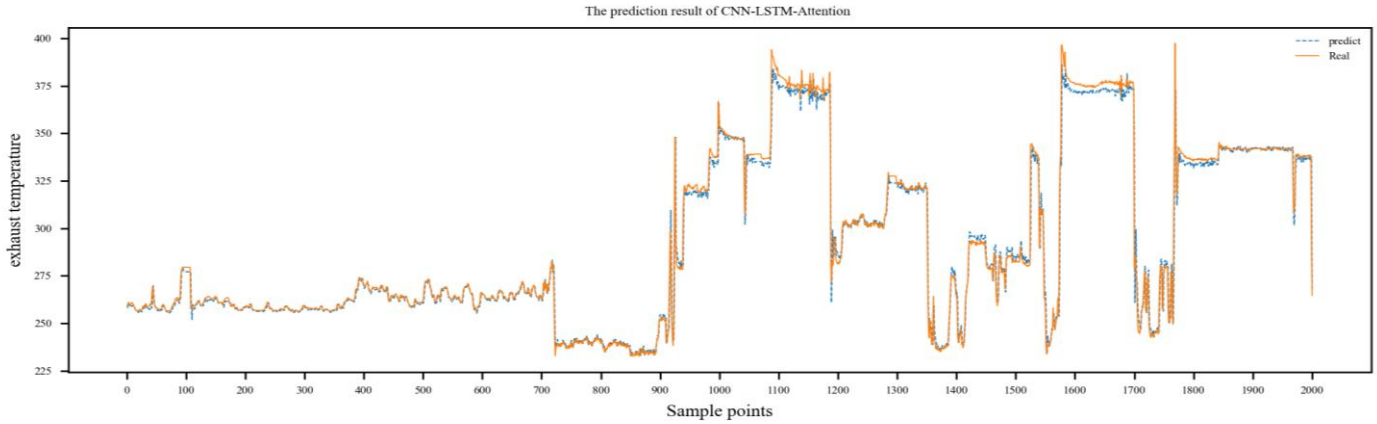

(a) 1 step of CNN-LSTM-Attention prediction

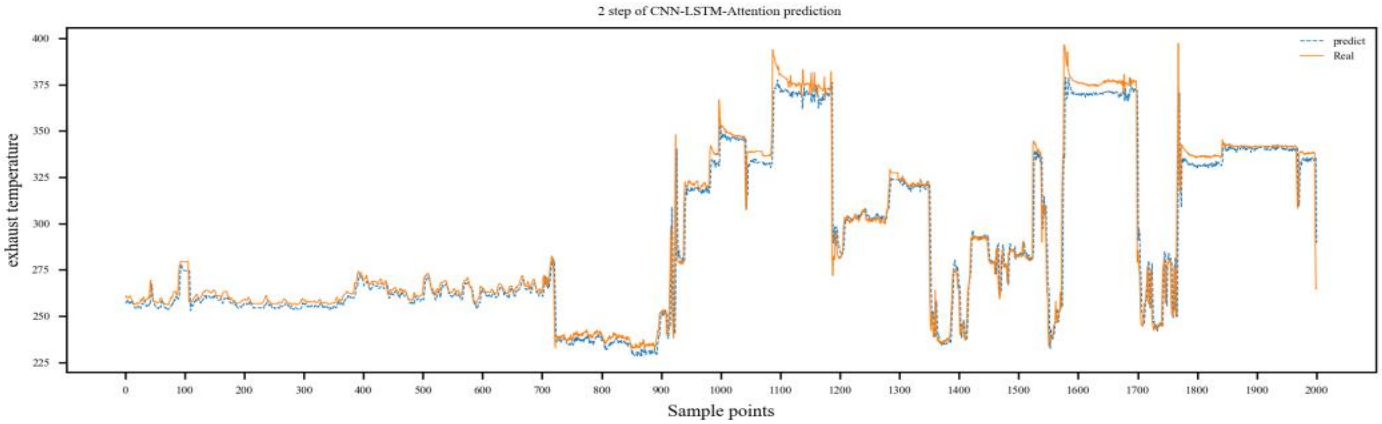

(b) 2 step of CNN-LSTM-Attention prediction

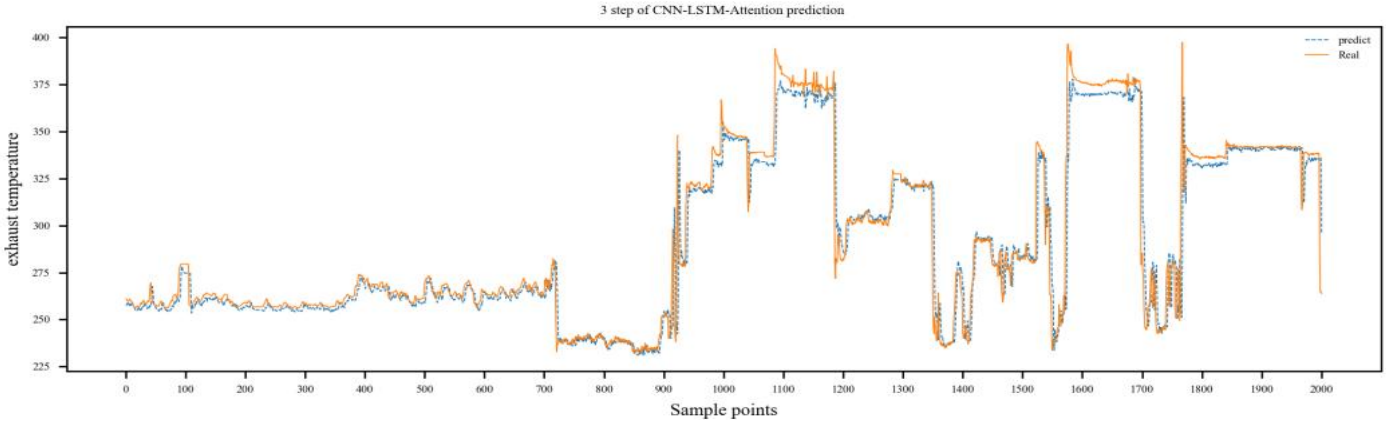

(c) 3 step of CNN-LSTM-Attention prediction

Fig. 7 Effect of output prediction step on the alignment between predicted and actual values.

The corresponding evaluation metrics for different output steps are summarized in Table 5.

Table 5 Performance metrics under varying output prediction step sizes.

Output Step	MAE	MAPE (%)	MSE	RMSE	R^2
1	3.9944	1.3481	39.6038	6.2932	0.9805
2	5.4821	1.8920	135.4269	11.6373	0.9333
3	6.6595	2.3049	183.7696	13.5561	0.9094

As shown in Table 5, increasing the output step size leads to a rise in MAE, MSE, MAPE, and RMSE values, while the R^2 decreases. Therefore, an output step of 1 was selected as the optimal configuration to ensure the best prediction accuracy. Following the hyperparameter tuning procedure described above, the finalized optimal values for the CNN-LSTM-Attention model are summarized in Table 6.

Table 6 Optimal hyperparameter settings for the CNN-LSTM-Attention model.

Parameter Category	Hyperparameter	Candidate Values	Optimal Value
Input Layer	Input time step	[5, 10, 15]	5
CNN Layer	Number of filters	[16, 32, 64, 128]	32
	Kernel size	[1, 2, 3]	2
	Activation function	—	ReLU
	Pooling size	[1, 2, 3]	2
LSTM Layer	Number of LSTM units	[16, 32, 64, 128]	64
	Dropout rate	[0.1, 0.2, 0.3]	0.2
	LSTM activation function	—	Sigmoid
Attention Layer	Attention activation	—	Softmax
Output Layer	Output prediction step	[1, 2, 3]	1
	Optimizer	—	Adam
	Batch size	[16, 32, 64, 128]	32
	Epochs	[100, 200, 300, 400, 500]	300

3.5 Comparative Analysis of Prediction Results

The CNN-LSTM-Attention model, configured with the optimal hyperparameters as outlined in Table 6, was employed to predict the cylinder exhaust temperature using the refined dataset developed in Section 3.3. The model's training and testing performance is depicted through loss curves shown in Figure 8.

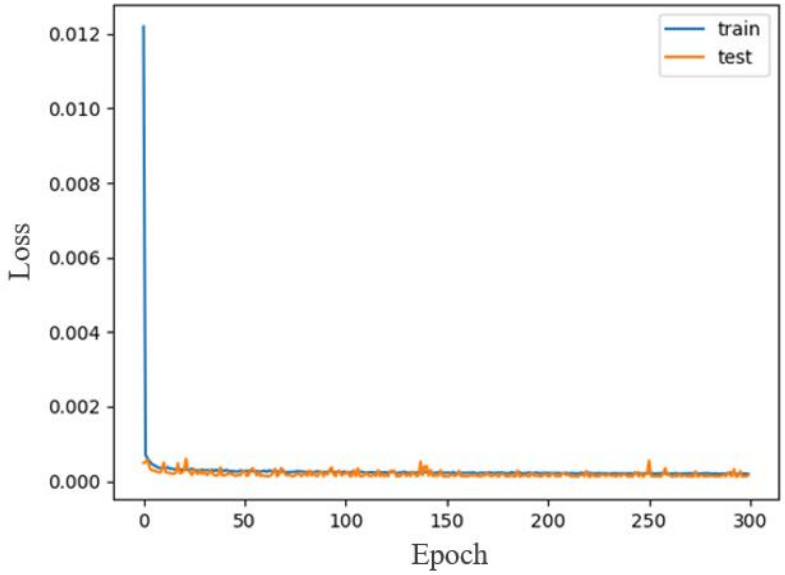

Fig. 8 Training and testing loss curves for the CNN-LSTM-Attention model.

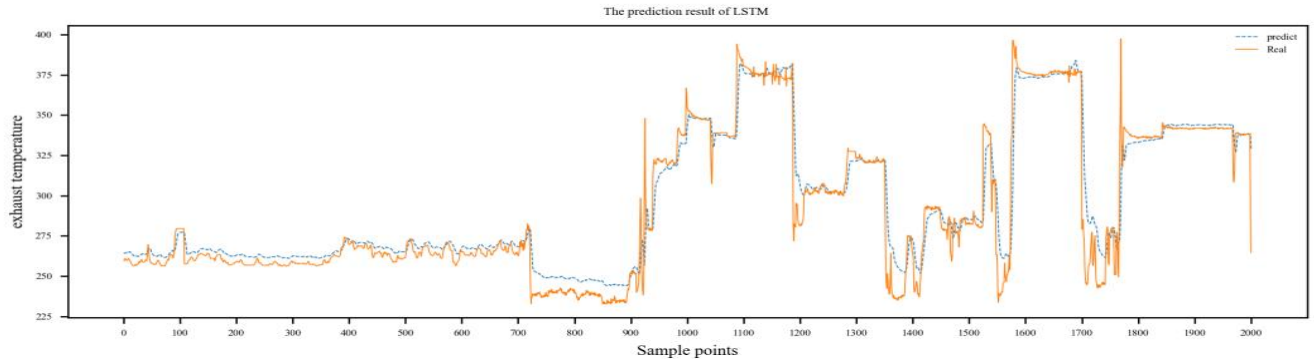

(a) The prediction result of LSTM

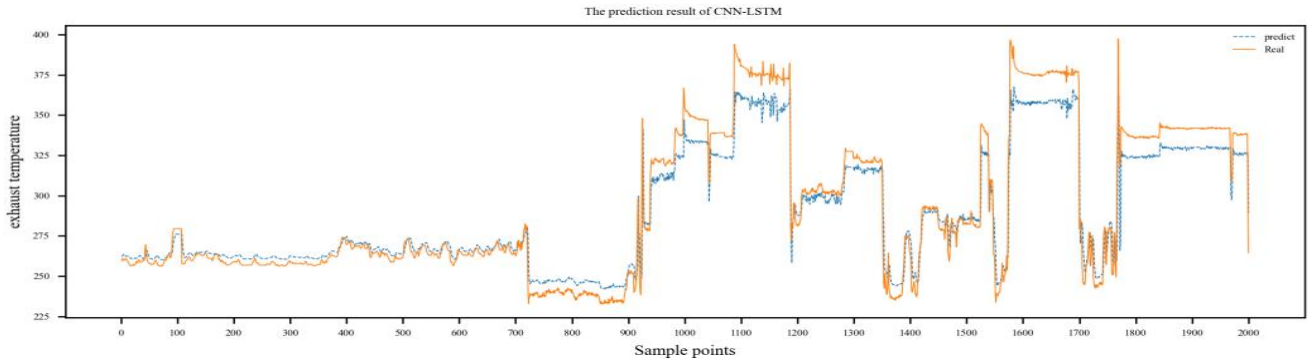

(b) The prediction result of CNN-LSTM

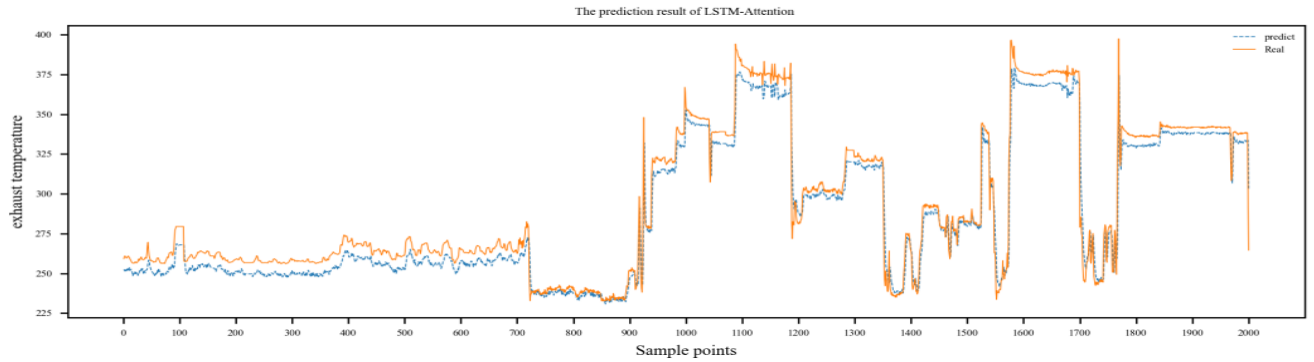

(c) The prediction result of LSTM-Attention

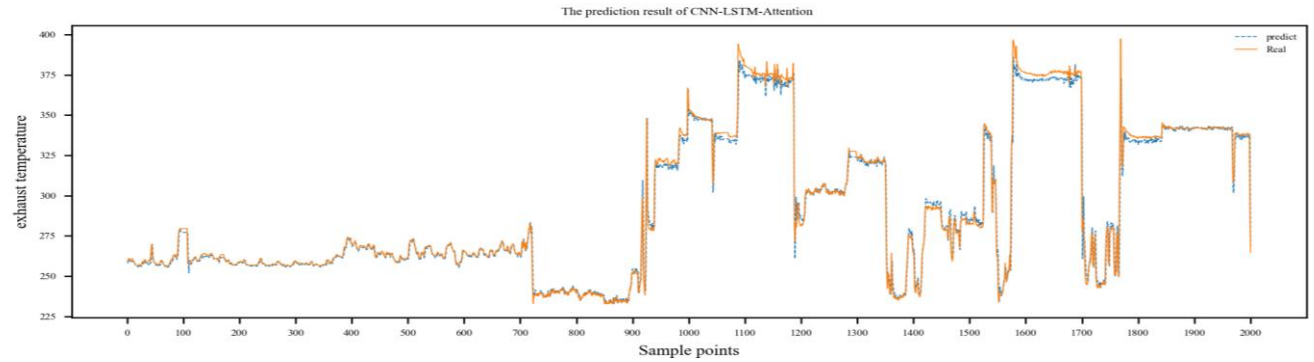

(d) The prediction result of CNN-LSTM-Attention

Fig. 9 Comparison of predicted and actual cylinder exhaust temperature across four models.

As illustrated in Figure 8, the training loss exhibits a steep initial decline, indicating rapid learning during the early epochs. During the intermediate training phase, both training and testing loss curves converge and stabilize near zero, suggesting that the model has effectively generalized to unseen data. The testing loss closely tracks the training loss throughout, with no observable divergence - indicating an absence of overfitting. In the final phase, the loss remains consistently low with only minor fluctuations, likely resulting

from inherent noise in the dataset. These observations affirm the model's learning stability, robust convergence, and high predictive accuracy.

To benchmark the performance of the proposed model, a comparative analysis was conducted against three alternative deep learning models: LSTM, CNN-LSTM, and LSTM-Attention. The predicted exhaust temperature curve generated by each model were compared with the actual values, as illustrated in Figure 9.

While all four models demonstrate the ability to approximate the general trend of cylinder exhaust temperature, notable performance differences were observed. The LSTM model can capture the overall trend of the data. However, it often produces excessively smooth predictions. As a result, it becomes less sensitive to short-term changes and may miss potential anomalies. The CNN-LSTM and LSTM-Attention models generally follow the same trend as the actual values. Both show improved prediction accuracy compared to the standard LSTM model. However, they still exhibit noticeable deviations between the predicted and actual curves, leading to lower overall alignment.

In contrast, the CNN-LSTM-Attention model displays the highest degree of congruence with the actual data, effectively capturing both global patterns and local variations. A quantitative comparison of model performance, based on standard evaluation metrics, is summarized in Table 7.

Table 7 Quantitative evaluation of model performance using error metrics.

Model	MAE	MAPE (%)	MSE	RMSE	R^2
LSTM	6.7338	2.4428	144.5594	12.0233	0.9288
CNN-LSTM	8.3278	2.6982	121.2235	11.0102	0.9403
LSTM-Attention	6.9770	2.4011	79.4905	8.9157	0.9608
CNN-LSTM-Attention	3.9944	1.3481	39.6038	6.2932	0.9805

The CNN-LSTM model, through the addition of convolutional layers, improves the extraction of spatial features from raw sensor data. Compared to the LSTM model, it reduces MSE and RMSE by 23.34 and 1.01, respectively, and achieves a closer R^2 value to 1. However, slight increases in MAE and MAPE are observed. The LSTM-Attention model further improves sensitivity to temporal dependencies, reducing MSE by 65.07, RMSE by 3.11, and MAPE by 0.04, albeit with a marginal increase in MAE.

The proposed CNN-LSTM-Attention model synthesizes the benefits of convolutional feature extraction, recurrent temporal learning, and attention-driven context awareness. It achieves the best performance across all evaluation indicators, yielding the lowest prediction errors and highest forecast accuracy among the models tested.

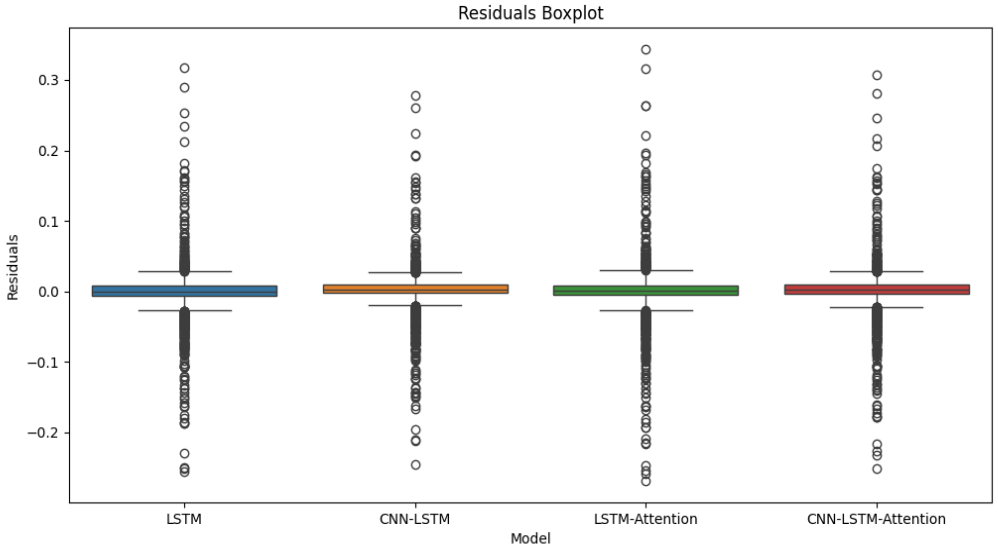

Fig. 10 Boxplot of residual distributions for all compared models.

To further assess model robustness, residual distribution [52] plots were generated for all four models and are presented in Figure 10. The residuals of the CNN-LSTM-Attention model are tightly clustered around zero, indicating minimal bias. Additionally, its interquartile range (IQR) is the smallest among the models, suggesting low variance in prediction errors. The model also demonstrates a reduced number of outliers, confirming its superior adaptability in handling anomalous or noisy samples.

In summary, the CNN-LSTM-Attention model outperforms both traditional and hybrid deep learning models (LSTM, CNN-LSTM, LSTM-Attention) across all major evaluation metrics. It demonstrates greater accuracy, stability, and generalization capability. So, it is particularly well-suited for high-precision intelligent monitoring of marine engine cylinder exhaust temperature.

4. Algorithm Optimization

To improve training efficiency and enhance prediction accuracy, this study incorporates Particle Swarm Optimization (PSO) into the CNN-LSTM-Attention model. PSO is applied to optimize key hyperparameters by performing a global search across the parameter space. When combined with the LSTM-based framework, it enables automatic tuning of critical settings such as input step size, the number of LSTM units, and the number of training epochs. Through iterative particle updates, PSO identifies the most effective parameter combinations and then optimizes the model structure in a systematic and adaptive way. This approach overcomes the limitations of manual or random hyperparameter selection commonly associated with LSTM networks. It also streamlines the tuning process, reduces training complexity, and lowers the risk of overfitting. As a result, the predictive performance and robustness of the hybrid model are notably enhanced.

In the PSO algorithm [53], each particle represents a candidate solution in the hyperparameter space and adjusts its position based on its personal best experience and the global best solution found by the swarm. This collaborative mechanism ensures systematic exploration and accelerated convergence toward an optimal configuration. The theoretical workflow of the PSO-augmented optimization procedure is illustrated in Figure 11.

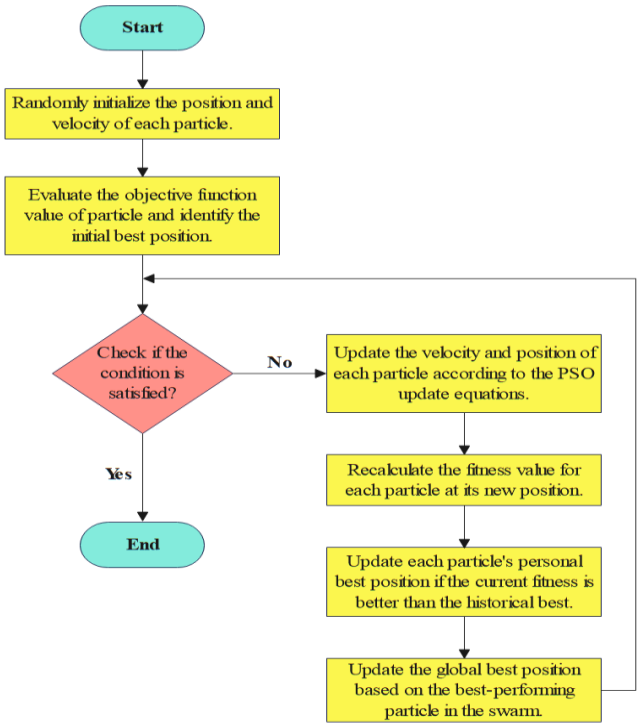

Fig. 11 Schematic diagram of PSO optimization algorithm flow.

The inclusion of PSO [54] provides a fast and effective way to optimize hyperparameters. It helps overcome the limitations of manual tuning and random initialization commonly found in traditional LSTM

models. It simplifies the tuning process, reduces model training complexity, and mitigates the risk of overfitting. As a result, the training performance is significantly improved, and the model's predictive accuracy is further enhanced.

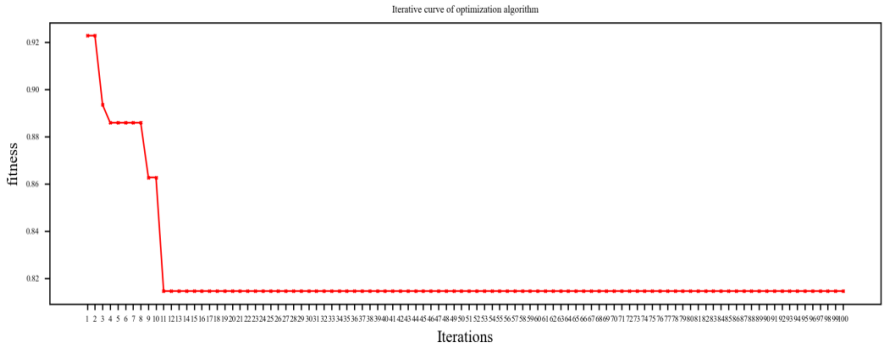

Fig. 12 Fitness curve of the PSO-optimized CNN-LSTM-Attention algorithm over 100 iterations.

As shown in **Error! Reference source not found.**, the PSO-optimized model achieves a stable fitness v alue after only 11 iterations, reflecting rapid convergence. Compared to the unoptimized baseline, the optimized model requires fewer iterations and demonstrates improved accuracy in predicting exhaust temperature trends.

Upon completion of PSO optimization, the model outputs suggested hyperparameter settings based on the global best particle. In contrast to conventional manual tuning, the PSO-enhanced model significantly streamlines the optimization process, reducing both development time and computational resources.

The optimal parameters obtained include:

(a) Learning rate: 0.002.

(b) Number of LSTM units: 38.

(c) CNN kernel size: 2.

(d) Number of training epochs: 68.

To facilitate a direct and intuitive comparison between the prediction performance of the model before and after PSO, both versions of the CNN-LSTM-Attention algorithm were executed using the same dataset. The respective prediction curves were superimposed onto a single plot and evaluated against the ground truth data. This comparative analysis is illustrated in Figure 13. In addition, a quantitative evaluation of prediction errors was conducted for both models, with the results summarized in Table 8.

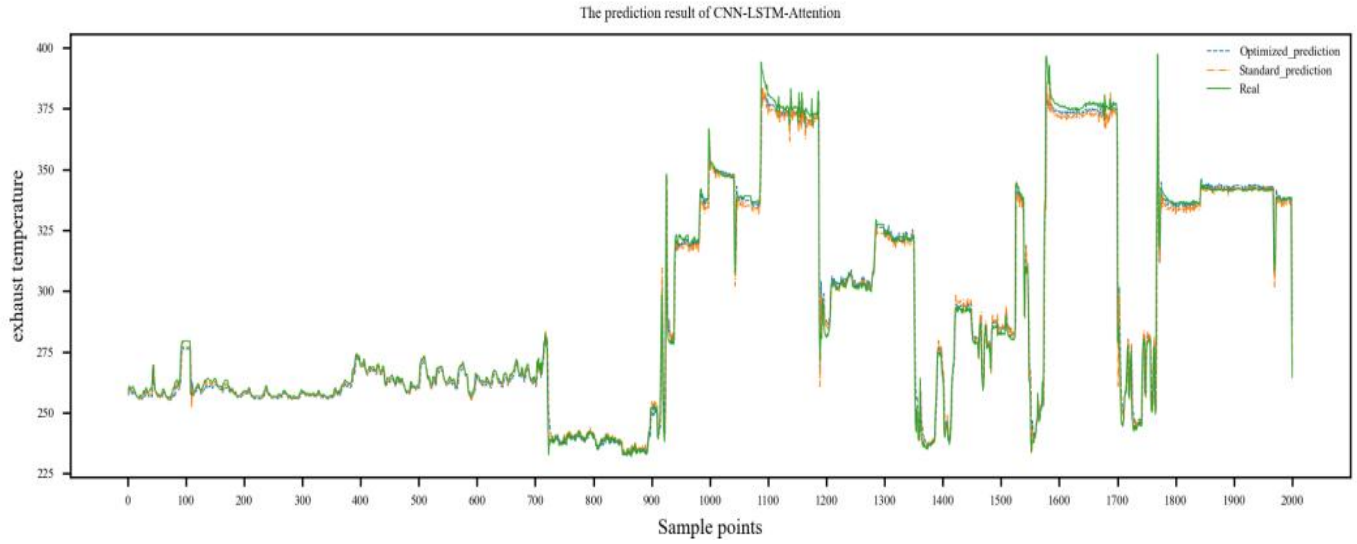

Fig. 13 Comparison of prediction results before and after PSO optimization.

As shown in Figure 13, both models exhibit prediction trends that generally follow the actual exhaust temperature curve (indicated in green). However, the prediction curve of the unoptimized model (represented in orange) shows more pronounced deviations from the ground truth, with multiple segments diverging significantly. In contrast, the PSO-optimized model (depicted in blue) demonstrates a notably closer alignment with the actual values, confirming an improvement in forecast accuracy following the optimization process.

Table 8 Performance comparison of the CNN-LSTM-Attention model before and after PSO optimization.

Model	MAE	MAPE (%)	MSE	RMSE	R^2
CNN-LSTM-Attention	3.9944	1.3481	39.6038	6.2932	0.9805
PSO-CNN-LSTM-Attention	2.4513	0.8141	25.2295	5.0229	0.9882

A more detailed examination of the error metrics presented in Table 8 further supports this conclusion. While the baseline CNN-LSTM-Attention model already achieved commendable predictive performance prior to optimization, the application of PSO led to measurable enhancements across all evaluated indicators. Specifically, the MAE decreased by 1.5431, the MSE was reduced by 14.3743, and the MAPE declined by 0.534 %. Additionally, the R^2 moved even closer to 1, indicating improved model fit and reduced variance between predicted and actual values.

In conclusion, the integration of PSO significantly enhanced the predictive capability of the CNN-LSTM-Attention model. The optimized architecture demonstrated reduced forecasting error and improved generalization across different operating conditions. These advancements are particularly effective in capturing the fluctuating trends of cylinder exhaust temperature, thereby reinforcing the model's practical value for intelligent condition monitoring of marine diesel engines.

5. Conclusions

This study presents a deep learning-based model for predicting the cylinder exhaust temperature of the No. 1 engine onboard an intelligent vessel. The proposed architecture integrates Convolutional Neural Networks, Long Short-Term Memory networks, and an Attention mechanism. The model was trained using real-world data collected from actual ship operations, ensuring practical relevance and robustness.

The CNN component enables effective extraction of spatial features, while the LSTM module captures temporal dependencies. The Attention mechanism further enhances the model by selectively emphasizing key features. As a result, the model produced accurate and stable prediction outcomes. In terms of MAE, the CNN-LSTM-Attention model demonstrates significant improvements over alternative methods. Compared to the LSTM, CNN-LSTM, and LSTM-Attention models, the MAE is reduced by 2.7394, 4.3334, and 2.9826, respectively. After further optimization using PSO, the model delivers more accurate exhaust temperature forecasts. By adjusting critical training parameters, such as step size and the number of LSTM units, the enhanced model reduced the MAPE to 0.8141 % and the RMSE to 5.0229. These improvements demonstrate a significant reduction in prediction error and confirm the model's enhanced accuracy and robustness in forecasting exhaust gas temperature trends.

A major advantage of this research is the use of real voyage data. Data were collected directly from onboard sensors. Unlike simulated data, real data include noise and fluctuations caused by changing sea conditions. This helped the model learn to handle irregular patterns and unpredictable inputs. The optimized CNN-LSTM-Attention model could accurately forecast cylinder exhaust temperature. It worked well even when the data were affected by environmental and operational disturbances. This makes the model suitable for real-time monitoring and early warning in ship engine systems [55].

However, this study still presents certain limitations that warrant further improvement. For instance, the dataset used in this work only covers a specific operational period of the marine diesel generator under relatively ideal conditions. In actual maritime operations, sensor-acquired data are often vast and influenced by varying sea states and dynamic operational conditions, which inevitably introduce prediction uncertainties.

Moreover, the subject vessel is a newly built intelligent ship, and its machinery remains within the optimal performance period. As a result, no significant anomalies or fault events were recorded during the monitoring timeframe. To further enhance the scientific value and practical relevance of this research, future studies may incorporate fault-related data and explore the integration of early warning mechanisms or conduct remaining useful life (RUL) prediction for critical marine components.

Looking toward to the future work, the proposed model shows strong potential for integration into autonomous control systems. It can also be linked with data-driven optimization frameworks to improve decision-making [56]. Such integration would enhance automation in ship operations. It would also reduce dependence on manual inspection and diagnostic tasks. These improvements support the shift toward fully intelligent and autonomous marine vessels. As a result, this study contributes not only to engine fault prediction but also to the advancement of smart maritime technologies more broadly.

FUNDING

This research was funded by the National Natural Science Foundation of China National Major Research Instrument Development Project (grant number 62127806).

NOMENCLATURE

Symbol	Quantity Description
F_t	the forget gate
W_f	the weight matrix associated with the forget gate
h_{t-1}	the previous time step
x_t	input vector
b_f	the bias term for the forget gate
$\sigma(\cdot)$	the sigmoid activation function
$I(t)$	the input gate
W_i	the weight for the input gate
b_i	the bias for the input gate
$\tilde{C}_t$	the candidate memory vector
W_c	the weight for the candidate memory content
b_c	the parameters for the candidate memory content
C_t	the memory cell
O_t	the output gate
W_o	the weight matrix associated with the output gate
b_o	the bias for the output gate
h_t	the encoder hidden state
s_{t-1}	the decoder's previous hidden state
ϑ_a^T	the learnable weight vector
r_s	the Spearman correlation coefficient
n	the total number of observations
$\hat{y}_i$	the model's output for the $i-th$ predicted value
y_i	the actual measured value from sensor data for the $i-th$ sample
T_P	average cylinder exhaust temperature
T_1	lubricating oil inlet temperature

T_2	cylinder liner cooling water inlet temperature
T_3	cylinder liner cooling water outlet temperature
T_4	turbocharger exhaust inlet temperature
T_5	turbocharger exhaust outlet temperature
P_1	fuel inlet pressure
P_2	lubricating oil inlet pressure
N_1	engine speed
N_2	turbocharger speed

ABBREVIATIONS

CNN	Convolutional Neural Network
LSTM	Long Short Term Memory
PSO	Particle Swarm Optimization
ReLU	Rectified Linear Unit
MAE	Mean Absolute Error
MAPE	Mean Absolute Percentage Error
MSE	Mean Square Error
RMSE	Root Mean Square Error
R^2	the Coefficient of Determination
IQR	Interquartile Range
RUL	Remaining Useful Life

REFERENCES

[1] Zhang, W., Zhang, Y., 2023. Research on classification and navigational risk factors of intelligent ship. *Brodogradnja,* 74(4), 105-128. https://doi.org/10.21278/brod74406

[2] Zhang, P., Ma, Y., Chen, H., Liu, C., Wu, Z., 2024. The Development and Challenges of Intelligent Ship. In *International Conference on Artificial Intelligence and Autonomous Transportationl*, Singapore. https://doi.org/10.1007/978-981-96-3973-1_17

[3] Soori, M., Arezoo, B., Dastres, R., 2023. Artificial intelligence, machine learning and deep learning in advanced robotics, a review. *Cognitive Robotics,* 3, 54-70. https://doi.org/10.1016/j.cogr.2023.04.001

[4] Pan, W., Xie, X.-l., He, P., Bao, T.-t., Li, M., 2021. An automatic route design algorithm for intelligent ships based on a novel environment modeling method. *Ocean Engineering,* 237, 109603. https://doi.org/10.1016/j.oceaneng.2021.109603

[5] Song, Y., Cao, X., 2024. Review of Intelligent Ship Path Planning Algorithms. *Frontiers in Management Science,* 3(1), 90-101. https://doi.org/10.56397/fms.2024.02.10

[6] Zhao, X., He, Y., Huang, L., Mou, J., Wen, J., Zhang, K., 2024. Adaptive collision avoidance decision system for autonomous ship navigation. *Journal of Marine Engineering & Technology,* 24(2), 132-146. https://doi.org/10.1080/20464177.2024.2443293

[7] Gao, J., Zhang, Y., 2024. Ship collision avoidance decision-making research in coastal waters considering uncertainty of target ships. *Brodogradnja,* 75(2), 75203. https://doi.org/10.21278/brod75203

[8] Theissler, A., Pérez-Velázquez, J., Kettelgerdes, M., Elger, G., 2021. Predictive maintenance enabled by machine learning: Use cases and challenges in the automotive industry. *Reliability Engineering & System Safety,* 215, 107864. https://doi.org/10.1016/j.ress.2021.107864

[9] Pookkuttath, S., Rajesh Elara, M., Sivanantham, V., Ramalingam, B., 2021. AI-Enabled Predictive Maintenance Framework for Autonomous Mobile Cleaning Robots. *Sensors (Basel),* 22(1), 13. https://doi.org/10.3390/s22010013

[10] Karatuğ, Ç., Arslanoğlu, Y., Soares, C.G., 2023. Review of maintenance strategies for ship machinery systems. *Journal of Marine Engineering & Technology,* 22(5), 233-247. https://doi.org/10.1080/20464177.2023.2180831

[11] Jian, L., Guo, J., Ma, H., 2022. Research on the Impact of Digital Innovation Driving the High-Quality Development of the Shipping Industry. *Sustainability,* 14(8), 4648. https://doi.org/10.3390/su14084648

[12] Liu, S., Chen, H., Shang, B., Papanikolaou, A., 2022. Supporting Predictive Maintenance of a Ship by Analysis of Onboard Measurements. *Journal of Marine Science and Engineering,* 10(2), 215. https://doi.org/10.3390/jmse10020215

[13] Wang, J., Cao, H., Cui, Z., Ai, Z., Jiang, K., 2023. Intelligent Fault Diagnosis of Marine Diesel Engines Based on Efficient Channel Attention-Improved Convolutional Neural Networks. *Processes,* 11(12), 3360. https://doi.org/10.3390/pr11123360

[14] Sun, J., Ren, H., Duan, Y., Yang, X., Wang, D., Tang, H., 2024. Fusion of Multi-Layer Attention Mechanisms and CNN-LSTM for Fault Prediction in Marine Diesel Engines. *Journal of Marine Science and Engineering,* 12(6), 990. https://doi.org/10.3390/jmse12060990

[15] Liu, B., Gan, H., Chen, D., Shu, Z., 2022. Research on Fault Early Warning of Marine Diesel Engine Based on CNN-BiGRU. *Journal of Marine Science and Engineering,* 11(1), 56. https://doi.org/10.3390/jmse11010056

[16] Ji, Z., Gan, H., Liu, B., 2023. A Deep Learning-Based Fault Warning Model for Exhaust Temperature Prediction and Fault Warning of Marine Diesel Engine. *Journal of Marine Science and Engineering,* 11(8), 1509. https://doi.org/10.3390/jmse11081509

[17] Han, P., Ellefsen, A.L., Li, G., Asoy, V., Zhang, H., 2021. Fault Prognostics Using LSTM Networks: Application to Marine Diesel Engine. *IEEE Sensors Journal,* 21(22), 25986-25994. https://doi.org/10.1109/jsen.2021.3119151

[18] M. Patil, M., M. Rekha, P., Solanki, A., Nayyar, A., Qureshi, B., 2022. Big Data Analytics Using Swarm-Based Long Short-Term Memory for Temperature Forecasting. *Computers, Materials & Continua,* 71(2), 2347-2361. https://doi.org/10.32604/cmc.2022.021447

[19] Liu, W., Cao, Y., 2025. Research on Offshore Vessel Trajectory Prediction Based on PSO-CNN-RGRU-Attention. *Applied Sciences,* 15(7), 3625. https://doi.org/10.3390/app15073625

[20] Lazakis, I., Dikis, K., Michala, A.L., Theotokatos, G., 2016. Advanced Ship Systems Condition Monitoring for Enhanced Inspection, Maintenance and Decision Making in Ship Operations. *Transportation Research Procedia,* 14, 1679-1688. https://doi.org/10.1016/j.trpro.2016.05.133

[21] Karagiannidis, P., Themelis, N., 2021. Data-driven modelling of ship propulsion and the effect of data pre-processing on the prediction of ship fuel consumption and speed loss. *Ocean Engineering,* 222, 108616. https://doi.org/10.1016/j.oceaneng.2021.108616

[22] Gupta, P., Rasheed, A., Steen, S., 2022. Ship performance monitoring using machine-learning. *Ocean Engineering,* 254, 111094. https://doi.org/10.1016/j.oceaneng.2022.111094

[23] Su, S., Miao, Z., Zhao, Y., Song, N., 2024. Digitally twin driven ship cooling pump fault monitoring system and application case. *Brodogradnja,* 75(4), 75403. https://doi.org/10.21278/brod75403

[24] Karatuğ, Ç., Arslanoğlu, Y., 2020. Importance of early fault diagnosis for marine diesel engines: a case study on efficiency management and environment. *Ships and Offshore Structures,* 17(2), 472-480. https://doi.org/10.1080/17445302.2020.1835077

[25] Theodoropoulos, P., Spandonidis, C.C., Giannopoulos, F., Fassois, S., 2021. A Deep Learning-Based Fault Detection Model for Optimization of Shipping Operations and Enhancement of Maritime Safety. *Sensors (Basel),* 21(16), 5658. https://doi.org/10.3390/s21165658

[26] Kang, Y.-J., Noh, Y., Jang, M.-S., Park, S., Kim, J.-T., 2023. Hierarchical level fault detection and diagnosis of ship engine systems. *Expert Systems with Applications,* 213, 118814. https://doi.org/10.1016/j.eswa.2022.118814

[27] Karatuğ, Ç., Arslanoğlu, Y., 2022. Development of condition-based maintenance strategy for fault diagnosis for ship engine systems. *Ocean Engineering,* 256, 111515. https://doi.org/10.1016/j.oceaneng.2022.111515

[28] Shahid, S.M., Ko, S., Kwon, S., 2022. Real-time abnormality detection and classification in diesel engine operations with convolutional neural network. *Expert Systems with Applications,* 192, 116233. https://doi.org/10.1016/j.eswa.2021.116233

[29] Li, Z., Liu, F., Yang, W., Peng, S., Zhou, J., 2022. A Survey of Convolutional Neural Networks: Analysis, Applications, and Prospects. *IEEE Trans Neural Netw Learn Syst,* 33(12), 6999-7019. https://doi.org/10.1109/TNNLS.2021.3084827

[30] Alzubaidi, L., Zhang, J., Humaidi, A.J., Al-Dujaili, A., Duan, Y., Al-Shamma, O., Santamaria, J., Fadhel, M.A., Al-Amidie, M., Farhan, L., 2021. Review of deep learning: concepts, CNN architectures, challenges, applications, future directions. *J Big Data,* 8(1), 53. https://doi.org/10.1186/s40537-021-00444-8

[31] Ruan, D., Wang, J., Yan, J., Gühmann, C., 2023. CNN parameter design based on fault signal analysis and its application in bearing fault diagnosis. *Advanced Engineering Informatics,* 55, 101877. https://doi.org/10.1016/j.aei.2023.101877

[32] Ruan, D., Zhang, F., Gühmann, C., 2021. Exploration and effect analysis of improvement in convolution neural network for bearing fault diagnosis. *2021 IEEE International conference on prognostics and health management (ICPHM)*, 7-9 June, Detroit, Michigan, United States. https://doi.org/10.1109/ICPHM51084.2021.9486665

[33] Su, Y., Gan, H., Ji, Z., 2024. Research on Multi-Parameter Fault Early Warning for Marine Diesel Engine Based on PCA-CNN-BiLSTM. *Journal of Marine Science and Engineering,* 12(6), 965. https://doi.org/10.3390/jmse12060965

[34] Ma, A., Zhang, J., Shen, H., Cao, Y., Xu, H., Liu, J., 2025. Research on Fault Diagnosis of Marine Diesel Engines Based on CNN-TCN–ATTENTION. *Applied Sciences,* 15(3), 1651. https://doi.org/10.3390/app15031651

[35] Perumal, T., Mustapha, N., Mohamed, R., Shiri, F.M., 2024. A Comprehensive Overview and Comparative Analysis on Deep Learning Models. *Journal on Artificial Intelligence,* 6(1), 301-360. https://doi.org/10.32604/jai.2024.054314

[36] Shen, Z., Fan, X., Zhang, L., Yu, H., 2022. Wind speed prediction of unmanned sailboat based on CNN and LSTM hybrid neural network. *Ocean Engineering,* 254, 111352. https://doi.org/10.1016/j.oceaneng.2022.111352

[37] Tang, H., Zhu, R., Wan, Q., Ren, D., 2025. Short-term prediction of trimaran load based on data driven technology. *Brodogradnja,* 76(1), 76101. https://doi.org/10.21278/brod76101

[38] Gao, B., Xu, J., Zhang, Z., Liu, Y., Chang, X., 2024. Marine diesel engine piston ring fault diagnosis based on LSTM and improved beluga whale optimization. *Alexandria Engineering Journal,* 109, 213-228. https://doi.org/10.1016/j.aej.2024.08.075

[39] Zhang, Y., Xin, D., 2020. Dynamic Optimization Long Short-Term Memory Model Based on Data Preprocessing for Short-Term Traffic Flow Prediction. *IEEE Access,* 8, 91510-91520. https://doi.org/10.1109/access.2020.2994655

[40] Al Hamoud, A., Hoenig, A., Roy, K., 2022. Sentence subjectivity analysis of a political and ideological debate dataset using LSTM and BiLSTM with attention and GRU models. *Journal of King Saud University - Computer and Information Sciences,* 34(10), 7974-7987. https://doi.org/10.1016/j.jksuci.2022.07.014

[41] Brauwers, G., Frasincar, F., 2023. A General Survey on Attention Mechanisms in Deep Learning. *IEEE Transactions on Knowledge and Data Engineering,* 35(4), 3279-3298. https://doi.org/10.1109/tkde.2021.3126456

[42] Wen, X., Li, W., 2023. Time Series Prediction Based on LSTM-Attention-LSTM Model. *IEEE Access,* 11, 48322-48331. https://doi.org/10.1109/access.2023.3276628

[43] Tang, J., Li, Y., Ding, M., Liu, H., Yang, D., Wu, X., 2022. An Ionospheric TEC Forecasting Model Based on a CNN-LSTM-Attention Mechanism Neural Network. *Remote Sensing,* 14(10), 2433. https://doi.org/10.3390/rs14102433

[44] Borre, A., Seman, L.O., Camponogara, E., Stefenon, S.F., Mariani, V.C., Coelho, L.D.S., 2023. Machine Fault Detection Using a Hybrid CNN-LSTM Attention-Based Model. *Sensors (Basel),* 23(9), 4512. https://doi.org/10.3390/s23094512

[45] Wan, A., Chang, Q., Al-Bukhaiti, K., He, J., 2023. Short-term power load forecasting for combined heat and power using CNN-LSTM enhanced by attention mechanism. *Energy,* 282, 128274. https://doi.org/10.1016/j.energy.2023.128274

[46] Chung, W.H., Gu, Y.H., Yoo, S.J., 2022. District heater load forecasting based on machine learning and parallel CNN-LSTM attention. *Energy,* 246, 123350. https://doi.org/10.1016/j.energy.2022.123350

[47] Xu, X., Yan, X., Yang, K., Zhao, J., Sheng, C., Yuan, C., 2021. Review of condition monitoring and fault diagnosis for marine power systems. *Transportation Safety and Environment,* 3(2), 85-102. https://doi.org/10.1093/tse/tdab005

[48] van den Heuvel, E., Zhan, Z., 2022. Myths About Linear and Monotonic Associations: Pearson's r, Spearman's ρ, and Kendall's τ. *The American Statistician,* 76(1), 44-52. https://doi.org/10.1080/00031305.2021.2004922

[49] Schober, P., Boer, C., Schwarte, L.A., 2018. Correlation Coefficients: Appropriate Use and Interpretation. *Anesthesia & Analgesia,* 126(5), 1763-1768. https://doi.org/10.1213/ANE.0000000000002864

[50] Gu, Z., 2022. Complex heatmap visualization. *Imeta,* 1(3), e43. https://doi.org/10.1002/imt2.43

[51] Ozsari, I., 2023. Predicting main engine power and emissions for container, cargo, and tanker ships with artificial neural network analysis. *Brodogradnja,* 74(2), 77-94. https://doi.org/10.21278/brod74204

[52] Gerber, E.A.E., Craig, B.A., 2023. Residuals and diagnostics for multinomial regression models. *Statistical Analysis and Data Mining: The ASA Data Science Journal,* 17(1), e11645. https://doi.org/10.1002/sam.11645

[53] Jain, M., Saihjpal, V., Singh, N., Singh, S.B., 2022. An Overview of Variants and Advancements of PSO Algorithm. *Applied Sciences,* 12(17), 8392. https://doi.org/10.3390/app12178392

[54] Chen, Y., Xu, X., Zhu, L., Liu, K., Yuan, J., 2024. PSO-based Prediction Method for CNN-LSTM-Attention Networks. *4th International Conference on Communication Technology and Information Technology (ICCTIT)*, Guangzhou, China. https://doi.org/10.1109/ICCTIT64404.2024.10928510

[55] Stoumpos, S., Theotokatos, G., 2021. A novel methodology for marine dual fuel engines sensors diagnostics and health management. *International Journal of Engine Research,* 23(6), 974-994. https://doi.org/10.1177/1468087421998635

[56] Karatuğ, Ç., Arslanoğlu, Y., Guedes Soares, C., 2023. Design of a decision support system to achieve condition-based maintenance in ship machinery systems. *Ocean Engineering,* 281, 114611. https://doi.org/10.1016/j.oceaneng.2023.114611